A 16 × 16-Element Slot Array Fed by Double-Layered Gap Waveguide Distribution Network at 160 GHz

N.B. When citing this work, cite the original published paper.

(article starts on next page)

A 16 × 16-Element Slot Array Fed by Double-Layered Gap Waveguide Distribution Network at 160 GHz

XUHUI DING[1], **JIANPING AN**[1], (Member, IEEE), **XIANGYUAN BU**[1], **HANGCHENG HAN**[1], **JINLIN LIU**[2], (Member, IEEE), AND **ZHONGXIA SIMON HE**[2], (Senior Member, IEEE)

[1]School of Information and Electronics, Beijing Institute of Technology, Beijing 100081, China
[2]Microwave Electronics Laboratory, Department of Microtechnology and Nanoscience, Chalmers University of Technology, 41296 Gothenburg, Sweden

Corresponding authors: Hangcheng Han (hanhangcheng@bit.edu.cn) and Zhongxia Simon He (zhongxia@chalmers.se)

ABSTRACT In this article, a slot array with double-layered full-corporate-fed distribution network by ridge gap waveguide (RGW) in the G-band is presented. The array antenna proposed in this article contains 16 × 16-element radiation slots fed by air-filled ridge gap waveguide distribution network that achieves high-efficiency. Gap waveguide technology avoids the demand for perfect electrical contact in millimeter waves, therefore the expensive diffusion bonding and the laser welding processes are not demanded. Moreover, the high-accurate Computerized Numerical Control (CNC) machining is applied for the fabrication. Due to the limited layout space for the distribution network, two types of universal stepped cavity power dividers are presented in this article. The proposed array antenna is fed by a standard WR-5 waveguide at the bottom. Furthermore, the tested outcomes show that the proposed 16 × 16-element array has a gain larger than 30 dBi with over 50% antenna efficiency in the frequency range of 155-171 GHz.

INDEX TERMS Gap waveguide technology, slot array antenna, high-efficiency, 160 GHz.

I. INTRODUCTION

G-band (140-220 GHz) has been drawn considerable attention for imaging, sensing, and communication due to its short wavelength and wide available bandwidth [1]–[4]. For communication, wider bandwidth can enable tens of Gbps data rate transmission. More importantly, the size of antenna in this band is smaller than that of lower frequency bands, therefore more compact radio units can be built with ease of dense deployment.

Semiconductor technologies can only offer limited output power at such a high frequency band, therefore it is critical to enhance the antenna efficiency. The reflector and the lens antennas satisfy with the features of high-efficiency and high-gain. Nevertheless, because of the need for a focal length, it is very difficult to realize a planar geometries. Patch array antenna usually has very low cost and low profile. The dielectric substrate is often used to build planar array antennas, such as microstrip over the low-temperature co-firing ceramic (LTCC), substrate integrated waveguide (SIW), and printed circuit board (PCB). However, PCB based antennas suffer from high dielectric loss above 30 GHz [5]. For instance, various types of millimeter waves (mmWs) planar array antennas have been developed based on the SIW technology [7]–[17]. Especially, a few of hybrid planar array antennas of the LTCC technology and the SIW structure at 140 GHz have been reported in [18]–[21]. Although planar arrays realized by SIW, LTCC and microstrip technologies have advantage of the low-profile, large dielectric losses are unbearable in mmWs. Due to the aforementioned analysis, non-substrate wave-guiding structure is preferred for high-efficiency and high-gain array above 100 GHz. Thereby, a 32 × 32- and a 64 × 64-elements slot array fed by hollow waveguide that operates at 125 GHz have been reported in [22]. Both of them are characterized as properties of low-profile, high-efficiency and high-gain. However, the diffusion bonding technology is very expensive for the fabrication and complicated for the design.

In the past decade, a novel guiding geometry, gap waveguide [23] shows promising performances such as lower dielectric- and conductor-loss [24], flexible fabrication [25], and cost effectiveness in mmWs. Furthermore, for gap

---

The associate editor coordinating the review of this manuscript and approving it for publication was Chan Hwang See.

waveguide structures, the top of the metallic pins are built with a flat metallic plate with a tiny air gap between two geometries. If the height of the gap is smaller than quarter-wavelength of the operating frequency, a certain frequency stopband is generated from such a novel geometry. Most importantly, the frequency stopband is able to be operated by geometrical dimensions of the metallic pins and the embedded grooves or ridges between the metallic pins. On the other hand, the gap waveguide technology does not demand for promising electrical contact of the metallic plate and the posts wall in mmWs. Thereby, the complicated and expensive fabrication process in [22] is able to be avoided and gap waveguide geometries can be fabricated by die-sink electrical discharge machining, CNC machining or molding. In [26]–[29], various high-efficiency and high-gain arrays designed by ridge gap waveguide (RGW) in the V-band, E-band, and W-band have been reported. Another geometry, groove gap waveguide has also been explored to high-efficiency and high-gain arrays in V-band and W-band [30]–[34]. Moreover, gap waveguide technology can be applied for the passive element in mmWs because it does not require for good electrical contact [35]–[37]. According to the summary of the above references, the gap waveguide geometries characterize non-electrical contact, small conductor- and dielectric-losses compared with the traditional microstrip, hollow waveguide and SIW in mmWs. Nevertheless, additional studies and tests of gap waveguide geometries above 100 GHz have not been validated before. In this article, we propose a RGW-based corporate-fed planar slot array at 160 GHz to fill the gap. The major accomplishments of this article are stated as follows:

- Firstly, the current dimension of pins dropped to a considerable level so that it has become very challenging to adopt traditional CNC milling or molding technique to fabricate [23]. Usually, dry-etching or lithograph is the choice of the manufacture in such a high frequency band. Nevertheless, it is even more expensive than diffusion bonding technology. In this article, we have selected relatively bigger pins at 160 GHz so that CNC milling technology can be implemented on antenna fabrication.

- Secondly, according to the skin effect and the rough surface, the conductor loss of aluminum at 160 GHz is much greater than that in the low frequency band. This is also a big challenge for the high efficiency array design at 160 GHz. Therefore, the insertion loss of the antenna unit cells, the distribution network, and the other sending modules in this frequency band should be optimally designed so as to minimize the insertion loss to ensure the antenna efficiency.

The rest of this article is organized as follows. Section II focuses on the design of numerical geometries, such as the proper model of metallic pins, the array unit cell, power dividers and waveguide interface. The antenna array is measured in reflection coefficient, gain, radiation patterns and the cross polarization levels. The corresponding outcomes are presented in section III. Further analysis on measured gain
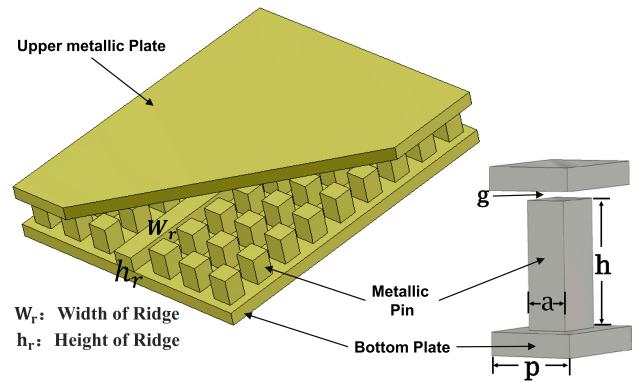

FIGURE 1. 3-D configuration of RGW for the array antenna in this article. Geometrical dimensions are shown in the figure: $p = 0.62$ mm, $a = 0.34$ mm, $W_r = 0.3$ mm, $h_r = 0.32$ mm, $h = 0.5$ mm and $g = 0.05$ mm.

and antenna efficiency are discussed in section IV. This paper is concluded in section V.

II. ANTENNA DESIGN
A. GEOMETRICAL DIMENSIONS OF THE METALLIC PINS
The principle of RGW can be analyzed through modeling it by two parallel plates, the upper layer is the ideal metallic plate layer and the bottom layer is the Artificial Magnetic Conductor layer, which is realized by the metallic pins. If the gap between PEC layer and the top surface of the metallic pins is less than a quarter of the wavelength corresponding to the current operating frequency, the RGW geometry prevents all TE and TM propagation modes over a wide stopband, however, a quasi-TEM mode along the ridge exists for desired frequency band signal propagation. A brief geometry of the RGW unit cell is shown in Fig. 1. In order that the array antenna can be fabricated by the CNC milling technology, the width of the metallic pins involved is carefully and appropriately chosen. The above frequency of $f_{ab} = 170$ GHz is assumed in this work. Therefore, by the previous standard pin size, the height of the pins should be chosen as $\lambda_0/4$, and the height of the metal pin is chosen as $h = 0.5$ mm. This selection makes it possible that the proposed antenna can be fabricated by CNC milling technology. Fig. 2 shows the calculated dispersion diagram of the RGW geometry by Eigenmode Solver with the stopband ranging from 80 to 225 GHz. The cutoff frequency of the quasi-TEM mode is about 110 GHz, and its whole bandwidth is from 110 to 225 GHz. The quasi-TEM mode is applied for wireless communications in the proposed array antenna, as depicted in Fig. 2.

B. ANTENNA SUB-ARRAY
Fig. 3 illustrates the configuration of the antenna unit cell from front- and back-views, which is designed as a 4 × 4-element using periodic boundary condition. Conventionally, the antenna unit cell in [27]–[34] is usually designed as a 2 × 2-element. Theoretically, the 2 × 2-element antenna unit cell in the G-band is geometrically too small so that the waveguide port in CST Microwave Studio is unable to be
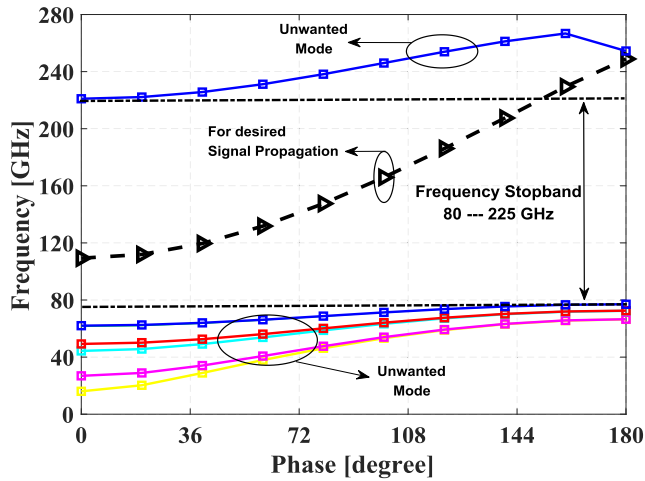
FIGURE 2. Numerically calculated dispersion diagram of the proposed RGW geometry by Eigenmode Method in Figure 1.
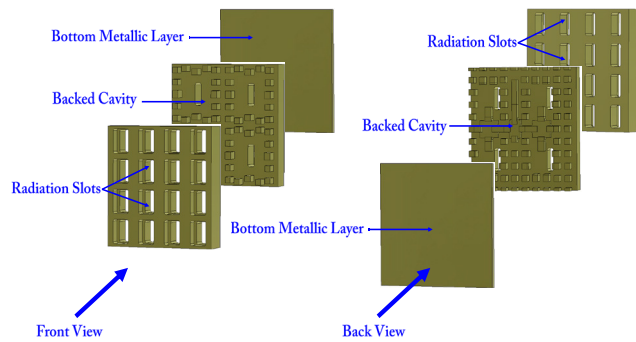

FIGURE 3. Exploded views for the 4 × 4-Element sub-array. Left-side: front view, and Right-side: back-view.

FIGURE 4. Geometrical dimensions for the proposed 4 × 4-Element sub-array. (a) Top radiation slots, (b) Front-view of middle layer — backed-cavity and (c) Back-view of middle layer — distribution network.

TABLE 1. Designed parameters of the 4 × 4-element sub-array depicted in Fig. 4.

W	6.2 mm	d	1.55 mm
W_{s1}	0.92 mm	L_{s1}	1.26 mm
W_{s2}	0.60 mm	L_{s2}	1.15 mm
W_b	2.00 mm	L_b	2.35 mm
W_c	0.37 mm	L_c	1.10 mm
W_f	1.37 mm	L_r	0.49 mm
L_f	1.15 mm		

accurately evaluated on the electromagnetic field based on gap waveguide structures. Thereby, a 4 × 4-element sub-array is modeled in this work, as shown in Fig. 3. The geometry of the present antenna unit cell is similar as that from the references [27]–[34]. The geometric structure primarily is made up of three layers: top radiation slots, middle backed-cavity, and the bottom distribution network. The radiation layer is the top layer of the entire sub-array, and it contains a radiation slots with a rectangular flare, whose function is to enhance its bandwidth. Under the radiation layer, the groove gap waveguide backed-cavity sets. Excited by a RGW feeding line, the electromagnetic fields are coupled to the cavity through a coupling hole in the middle of the sub-array. For fear of the misalignment errors that occur during assembly when the backed cavity and feedback layer are separated into two different layers, the distribution network layer sets on the backside of the backed-cavity layer. Therefore, a smooth metallic plate forms the bottom waveguide layer. Furthermore, the dimension between any two neighbored slots is evaluated to be 1.55 mm, equaling to $0.875\lambda_0$ which has the corresponding operating frequency of $f = 170$ GHz. The reason for selection for 1.55 mm is that the qualified radiation patterns can be obtained. Between different layers
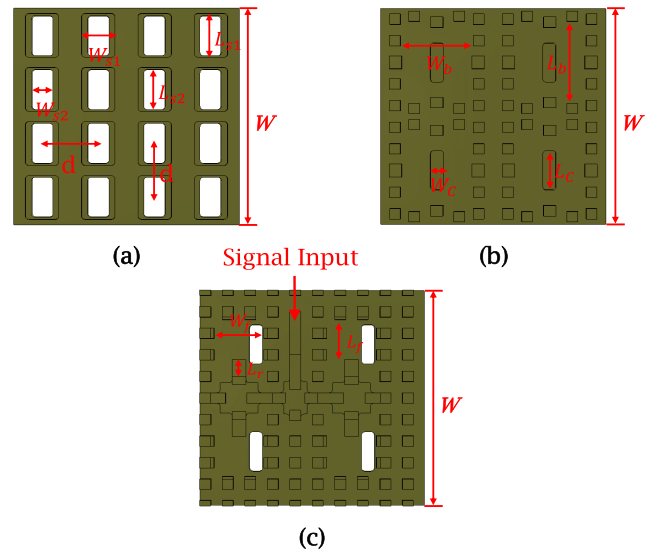
no electrical contact is demanded, as all three layers of the sub-array are separated by tiny gaps. The area of the designed 4 × 4-element sub-array is $6.2 \times 6.2\ mm^2$ on both vertical- and horizontal-planes in this paper. The geometrical dimensions of the antenna unit cell is depicted in Fig. 4, and Table 1 records the corresponding data. The numerical calculated E- and H-fields on the top layer of radiation slot are drawn in Fig. 5. Applying periodic boundary conditions, 16 × 16- element array performance is simulated. In Fig. 6, the blue solid line represents the reflection coefficient. As can be seen, over the frequency range of 153-170 GHz, a 10.52% relative bandwidth is achieved defined by a −10 dB return loss threshold. The red line indicates the calculated directivity of the 16 × 16-element array antenna (exclude distribution network). The numerically calculated antenna efficiency is above 90% from 153 to 171 GHz.

C. RGW FEED LINES
As illustrated in Fig. 4(c), the distribution network in this work utilizes only one row of metallic pins are used for isolating the ridge line and the radiation slot. Naturally, more rows of pins give more suppression of mutual coupling,
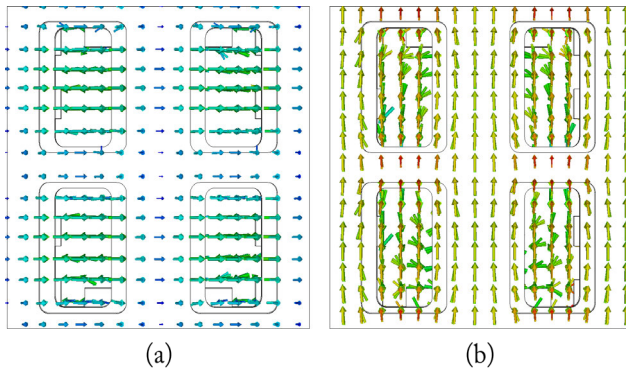
FIGURE 5. Configurations for fields distribution on the top of radiation slots at 160 GHz. (a) E-field. (b) H-field.
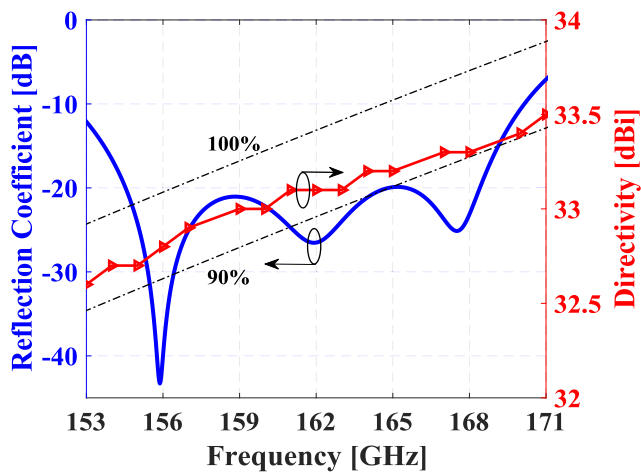

FIGURE 6. Numerically calculated reflection of the proposed 4 × 4-Element sub-array and the directivity of an array with 16 × 16-element slot using periodic boundary conditions.
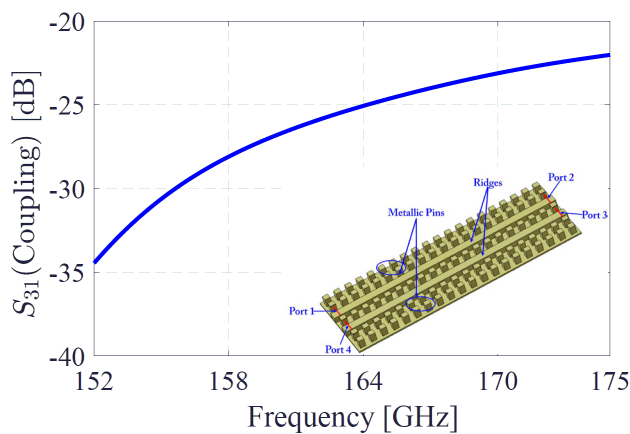

FIGURE 7. Numerically calculated mutual coupling between two parallel ridges separated by only one row of inductive posts. The top metallic smooth layer is hidden.

however, it is hard to implement due to a space constrain. To estimate coupling suppression with only single row of pins, a parallel ridge model is used as in Fig. 7. Simulation shows that the mutual coupling between two parallel

TABLE 2. Design parameters of two types of T-junction power dividers shown in Fig. 8.

L_{p1}	1.00 mm	L_{p2}	0.36 mm
P_o	0.4 mm	L_{sc1}	0.92 mm
W_{sc1}	0.64 mm	h_{sc1}	0.25 mm
L_{ex}	0.68 mm	L_{sc2}	0.87 mm
W_{sc2}	1.05 mm	h_{sc2}	0.25 mm

RGW lines, separated by one row of metallic pins, and the corresponding mutual coupling is below −20 dB from 152 to 175 GHz, which is a promising result at such high frequency.

In this article, two types of T-junction power dividers based on RGW are developed. As shown in Fig. 8, three T-junction power dividers have been applied for the 4 × 4-element sub-array. One T-junction power divider is with two metallic pins removed at output ports, and the other two are with only one metallic pin removed at output ports. These two types T-junction power dividers are different from those in [26]–[29], which are with continuous bend-ridges and difficult to be fabricated at 170 GHz. The 3-D configuration of the two types T-junction power divider is illustrated in Fig. 8. The corresponding geometries have been optimized so that the wide impedance bandwidth and the small reflection can be obtained. Fig. 9 and Fig. 10 depict the simulated input reflection coefficient in both amplitude and phase. Both reflection coefficients in amplitude are below −30 dB over a wide frequency band 152-175 GHz. The phases of output ports are identical. Compared with the T-junction power dividers introduced in [25]–[31], the proposed one characterizes compact, easy manufacture and even lower loss.

The whole array is excited by a standard G-band waveguide (WR-5) in the bottom layer. This transition part converts the electromagnetic fields through the rectangular waveguide into the RGW lines. The novel geometry works as the first power division stage and thereafter, makes the distribution network more compact. The topology of the proposed hybrid vertical transition divider is depicted in Fig. 11. In addition, since the dimensions of cross-sectional area of WR-5 is very small (1.3 mm×0.65 mm), the WR-5 waveguide has been fabricated by wire cutting technology. Fig. 12 shows the simulation performance results of the optimized vertical transition power divider. From 154 to 173 GHz, the input reflection coefficient is below −20 dB. Although the vertical transition power divider has a compact geometry, the two output ports have phase difference of 180 degree. In order to overcome the above problem, the feed networks on both sides of vertical transition power divider are mirrored, as depicted in Fig. 13. Fig. 14 depicts simulated E-field along the distribution network at 165 GHz. As shown in the figure, the phase uniformity of the distribution network is good. Then, the radiation patterns and gain can be guaranteed in this work.
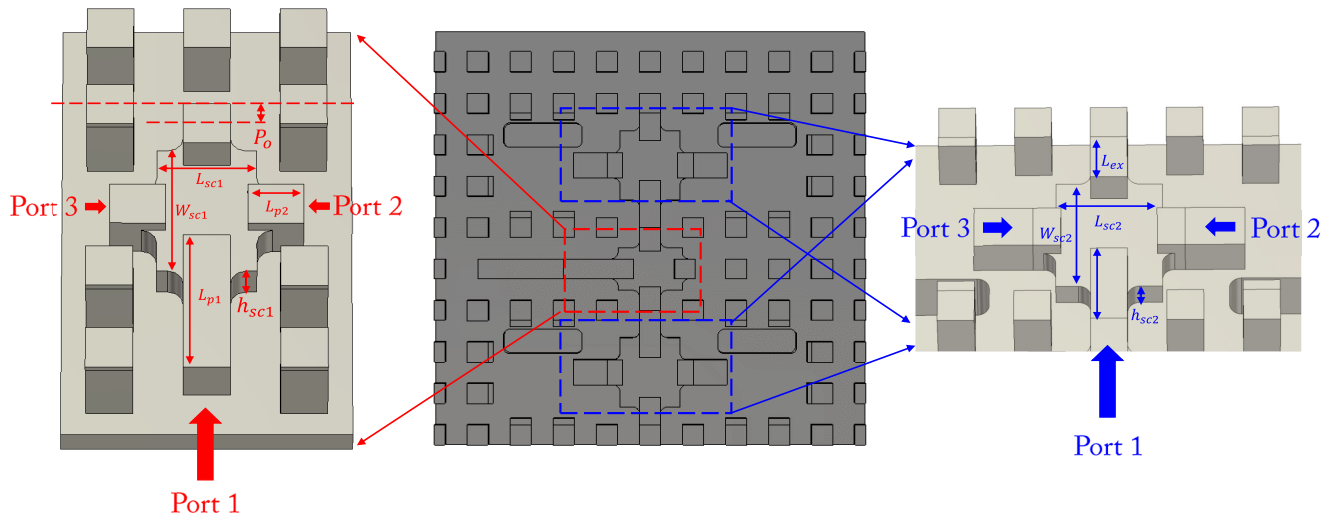
FIGURE 8. Two types of T-junction power dividers. Left-side: T-junction power divider with only one metallic pin removed at each output port. Right-side: T-junction power divider with two metallic pins removed at each output port. Top flat metallic plate is hidden so that the entire geometry is clearly illustrated. Geometrical dimensions are shown in the figure: P_o = 0.4 mm, W_o = 1.56 mm, L_{p1} = 0.71 mm, L_{p2} = 0.23 mm, L_{sc} = 0.87 mm, W_{sc} = 1.05 mm and h_{sc} = 0.25 mm.
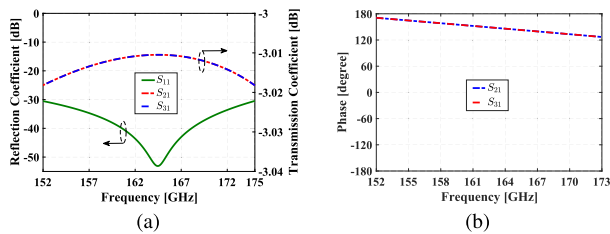
FIGURE 9. Numerical outcomes of the T-junction power divider with two metallic pins removed at output ports. (a) Amplitude. (b) Phase.
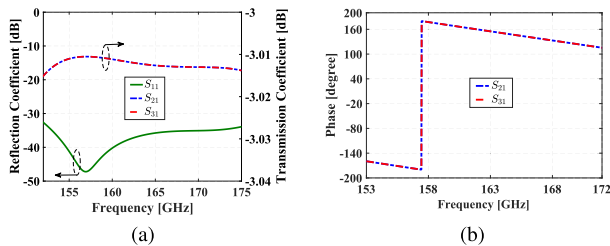

FIGURE 10. Numerical outcomes of the T-junction power divider with one metallic pins removed at output ports. (a) Amplitude. (b) Phase.

III. THE SIMULATION AND THE EXPERIMENT RESULTS OF THE ENTIRE ARRAY

The final structure of the manufactured array is shown in Fig. 15. As can be seen, the final geometrical size of the present array is 40 mm× 40 mm while the dimensions of the effective aperture are 24.8 mm ×24.8 mm. The total thickness is 8 mm. We have added extra 6 mm in order to connect the flange of PNA for the measurement. Thereby, the effective thickness of the present array is only 2 mm. The array antenna is fabricated using aluminum (Electric Conductivity 3.6×10⁷ S/m). The configuration of the whole array including holes for screws and guiding pins
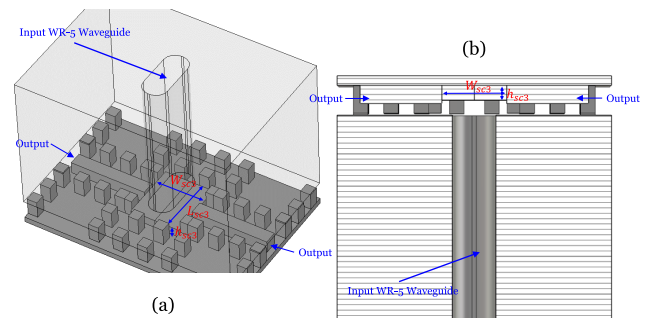

FIGURE 11. 3-D configurations of the vertical transition power divider. (a) 3-D Geometry. (b) E-plane cross-sectional view. Geometrical dimensions are shown in the figure: L_{sc3} = 1.60 mm, W_{sc3} = 1.32 mm and h_{sc3} = 0.31 mm.
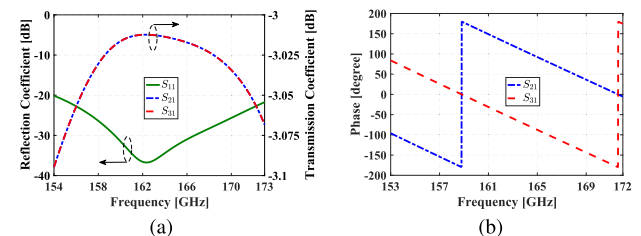

FIGURE 12. Numerically calculated outcomes of designed vertical transition from WR-5 to two RGW lines. (a) Amplitude. (b) Phase.

is presented in Fig. 15. The proposed antenna is thereby low-profile.

The entire structure of the array antenna is simulated by CST Microwave Studio, what is more, without any further optimization, the antenna reflection coefficient $|S_{11}| <$ −10 dB in the frequency range of 152-170 GHz, as depicted in Fig. 17. The realized reflection coefficient antenna has
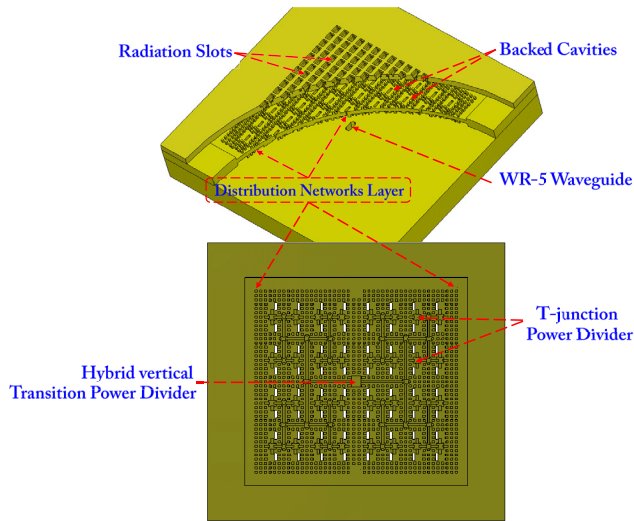
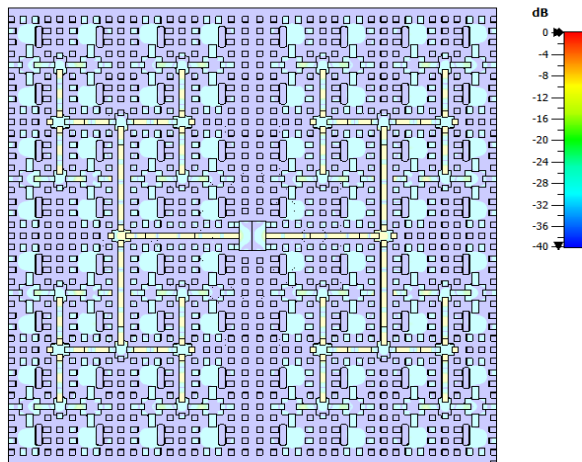**FIGURE 13.** Numerical configuration of the 16 × 16-element array in this work.

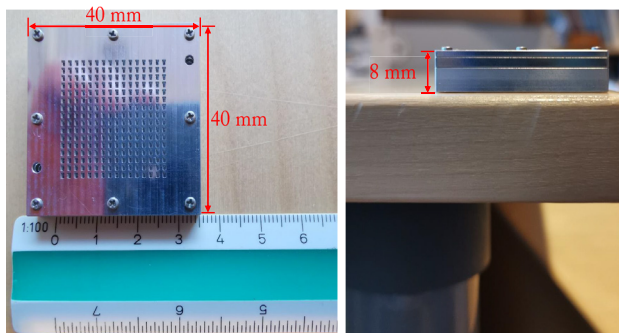**FIGURE 14.** Simulated E-field on the distribution network at 165 GHz.

FIGURE 15. The photograph of the final fabricated antenna.

FIGURE 16. Experimental setup for the reflection coefficient.
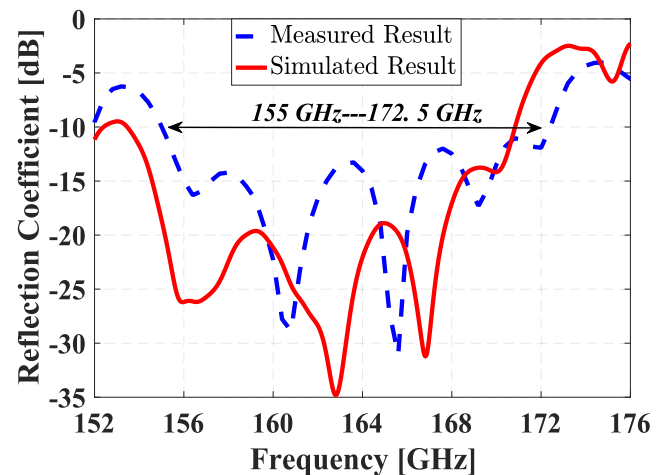
FIGURE 17. The numerical and the experimental reflection coefficients.

due to the manufacturing tolerances and misalignment of the three layers.

The radiation properties, such as gain, radiation patterns and cross-polarization levels, are tested in an anechoic chamber. The calculated and the experimental normalized radiation patterns of the 16 × 16-element array are plotted at three different frequencies of 158, 166, and 172 GHz, and the performance comparisons are shown in Figs. 18-19. The co-polar radiation patterns from the experiment show good identities of the calculated values. Meanwhile, the measured antennas E- and H-planes cross-polarization patterns are also presented, as can be seen, the cross-polarization values are greater than −35 dB in all planes. The proposed antenna

been experimentally tested by a Keysight PNA, as depicted in Fig. 16. However, the measured one is smaller than −10 dB from 155 to 172.5 GHz (10.2% input impedance bandwidth). As illustrated in Fig. 17, there is a small shift in the reflection coefficient to higher frequency. These discrepancies may be
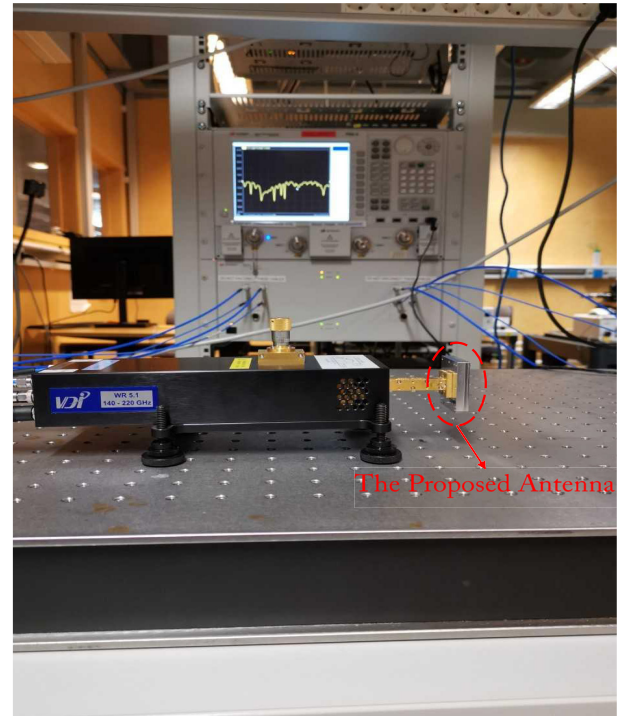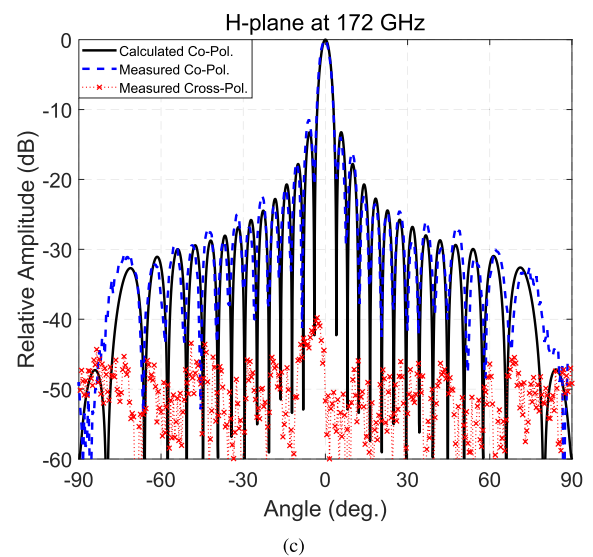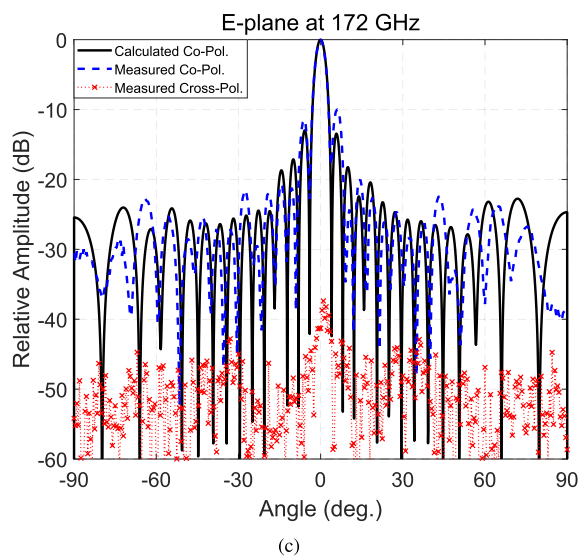
FIGURE 18. Radiation patterns from the calculation and the experiment on the E-plane: (a) 158 GHz, (b) 166 GHz and (c) 172 GHz.

FIGURE 19. Radiation patterns from the calculation and the experiment on the H-plane: (a) 158 GHz, (b) 166 GHz and (c) 172 GHz.

FIGURE 20. The calculated and the measured gain of the proposed array.

FIGURE 21. Simulated electric field distribution of a straightforward RGW transmission line at frequency 165 GHz. The top metallic plate is hidden so that the entire geometry is able to be clearly shown.

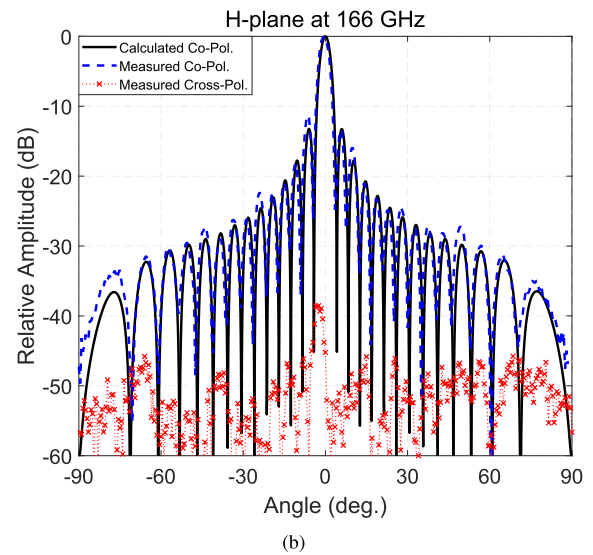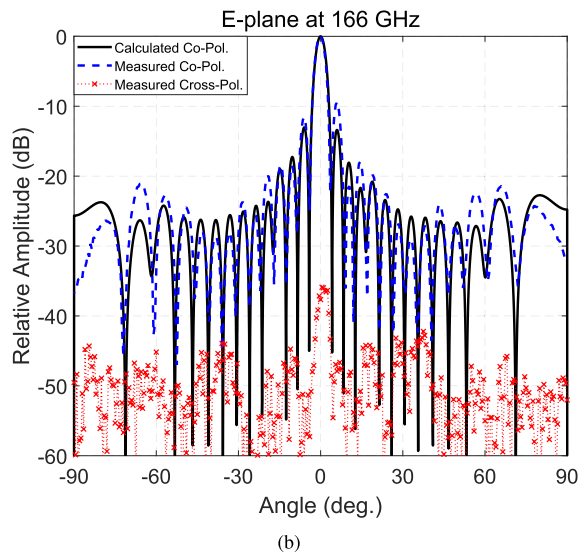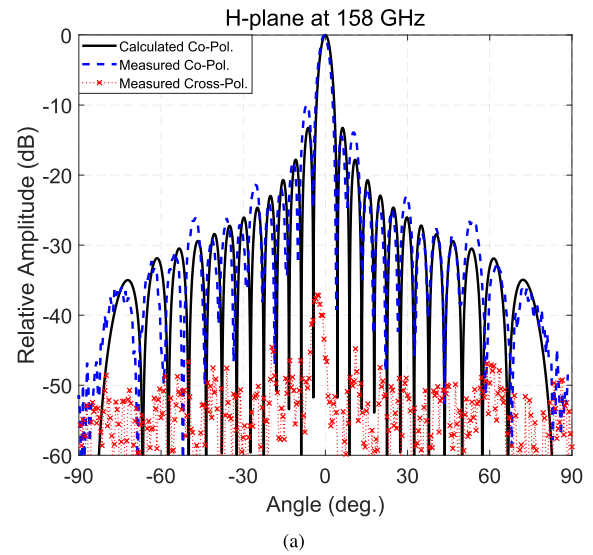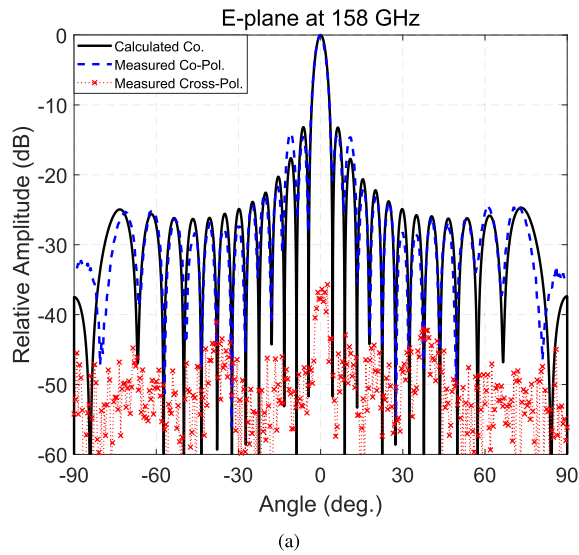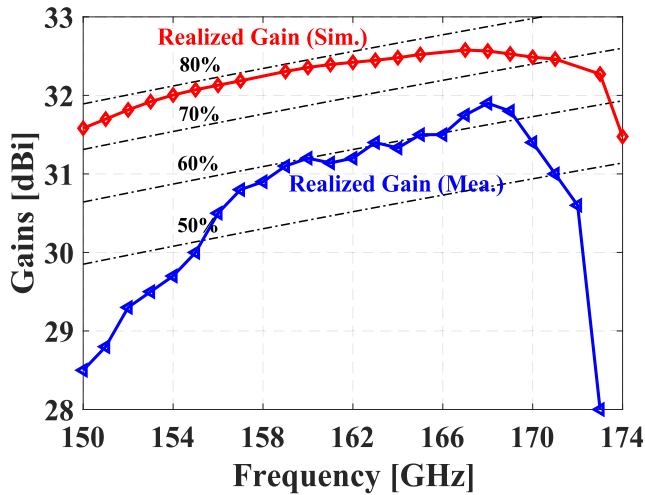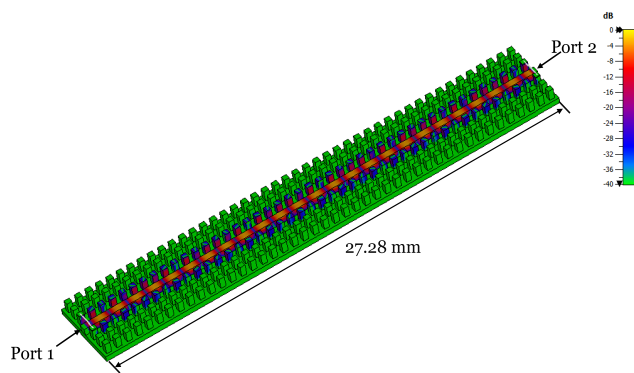**FIGURE 22.** Simulated transmission coefficients with different surface roughness values according to the model in Fig. 21.
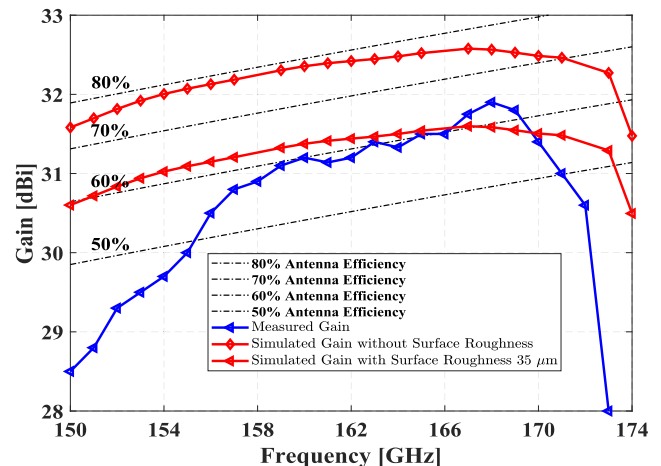
FIGURE 23. Comparison of the simulated gain, the measured and the simulated gain with the surface roughness of the proposed array.

exhibits an outstanding radiation pattern performance over the broad frequency range of 155-172 GHz.

Fig. 20 shows the simulated and measured gain results of the antenna in a specific frequency range (155-171 GHz). In the corresponding frequency range, the antenna gain is bigger than 30 dBi, and the antenna efficiency is more than 50%. The gain response is quite flat in operating frequency band. The difference between the simulated and measured gain results of the antenna's radiation pattern may be due to the additional reflection losses and extra ohmic losses caused by the reduced metal conductivity with surface roughness.

IV. DISCUSSION ABOUT THE MEASUREMENTS
Last section, we have mainly presented the reflection, the radiation patterns, the cross-polarization levels and the antenna gain of the proposed array. Nevertheless, there is a big difference between the numerical gain and the measured one. On the other hand, the measured antenna efficiency is around 60%, yet the calculated on is about 80%. For this appearance, there are probably three reasons.

Firstly, G-band (140-220 GHz) is a higher frequency band, and the corresponding skin depth of aluminum is merely

0.2072 μm. Thereby, the conductor loss in such a frequency band is much bigger than that value in V-band or E-band. In order to verify the conductor loss of RGW by aluminum in G-band, a simple straightforward RGW transmission line is built, as depicted in Fig. 21. The simulated transmission coefficients S_{21} are illustrated in Fig. 22. The model is first simulated with PEC material, and then is calculated again with aluminum. Thus, the difference from both calculations indicates the conductor loss of the geometry illustrated in Fig. 21. The simulated conductor loss here is about 0.2 dB/cm, which is much bigger than that in V-band.

Secondly, the inaccurate assembling of the proposed three-layered array is probably another reason for the drop of the gain and the efficiency. In [26], the effect from the misalignment of different layers has been researched. The outcome indicates that the misalignment within 60 μm is acceptable for the array antenna to obtain stable input impedance bandwidth and gain. Since the reflection coefficient and the

(a)

(b)

(c)

(d)

FIGURE 24. Surface roughness checking under a high resolution microscope: (a) top plate of vertical transition, (b) the T-junction power divider with two metallic pins remove at output ports, (c) the T-junction power divider with a metallic pin remove at output ports and (d) a straightforward RGW transmission line.
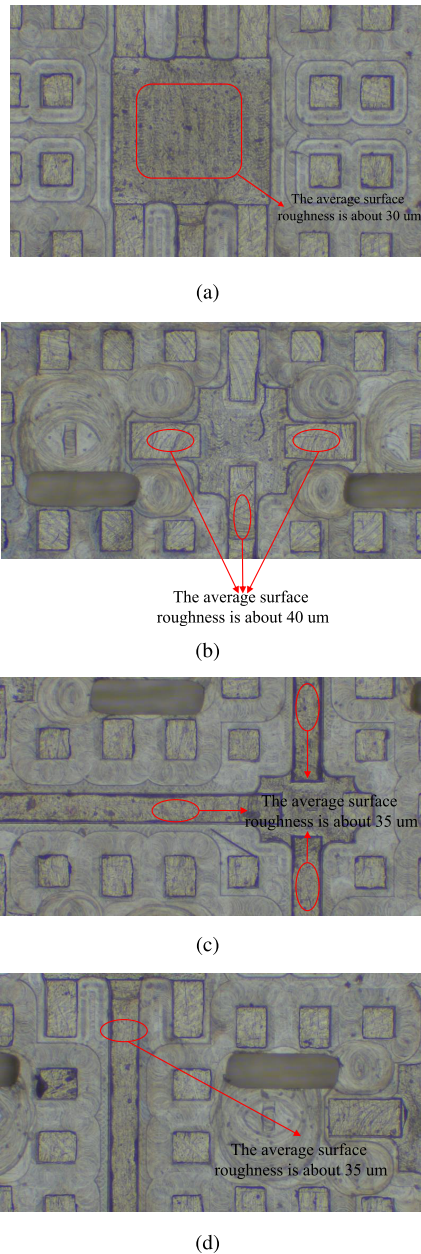
radiation patterns behave good in this work, the misalignment error should be much smaller than 60 μm.

More importantly, the surface roughness of the ridge and the bottom metallic plate play a key role for the drop of the antenna gain and the antenna efficiency. In order to search the surface roughness, the distribution layer has been checked under a high resolution microscope. As shown in Fig. 24, four parts from the distribution network layer have been carefully checked, such as the top metallic plate of vertical transition, two T-junction power dividers and a straightforward RGW transmission line. The average manufacture tolerance

TABLE 3. Conductor losses from the different surface roughness values.

Surface Roughness [μm]	Conductor Losses [dB/cm]
0	0.2
25	0.28
50	0.35
75	0.41

is about 35 μm. However, some big striations touched by the milling tool are clear, especially on the surface of the cavity parts. Then, the research for the conductor losses caused from the surface roughness has been done again. As depicted in Fig. 22, the simulated S_{21} caused by the surface roughness values 25 μm, 50 μm and 75 μm indicate that the conductor losses increase from 0.77 to 1.12 dB. The corresponding conductor loss per unit length are shown in Table 3, which records 0.28 dB/cm, 0.35 dB/cm and 0.41 dB/cm, respectively.

The antenna gain and the antenna efficiency are definitely affected by the surface roughness caused by the fabrication process. The surface roughness values checked from the microscope has been input again into the numerical model of 16 × 16 array. As illustrated in Fig. 23, the numerical antenna gain drops about 1 dB after inputting the surface roughness value 35 μm. Meanwhile, the corresponding antenna efficiency also decreases from 80% to 60% in the operating frequency band. This calculated value verifies the surface roughness value from the checking under microscope. Another minor reason, the misalignment, has not considered in this work.

As analyzed before, the conductor loss increases because of the skip effect in the high frequency band, the mechanical misalignment and the surface roughness. There are probably two solutions for the issue. Dry etching or electron beam technology is able to provide even more accurate manufacture process. However, both technologies are very expensive, and not suitable for the mass production. On the other hand, the conductor loss can be reduced by silver-plating on the surface of the array antenna since its conductivity has almost a factor two times larger than that value of aluminum. The later method is very helpful to improve the quality of the array in the high frequency band.

In brief, gap waveguide technology has been certified its advantages of low loss, easy fabrication and non-electrical contact from Ka-band to W-band in the past works [26]–[36]. In this work, a complicated array antenna fabricated by CNC-milling technology proves that gap waveguide technology still effectively works in the G-band (140-220 GHz). This work supplies a new choice for the passive components, antennas and RF-components packaging above 100 GHz except for conventional hollow waveguide and ridge waveguide.

V. CONCLUSION

In this paper, a RGW-based 16 × 16 corporate-feed array antenna in the G-band is proposed. The simplified structure

reduces the manufacturing costs, so it leads to broad application prospects in the future. The proposed slot waveguide antenna can be directly connected through the WR-5 waveguide port. The measurement result of the antenna gain is greater than 30 dBi from 155 GHz to 171 GHz, meanwhile, the efficiency of the antenna is greater than 50%.

REFERENCES

[1] S. M. Rahman, Z. Jiang, M. I. B. Shams, P. Fay, and L. Liu, "A G-band monolithically integrated quasi-optical zero-bias detector based on heterostructure backward diodes using submicrometer airbridges," *IEEE Trans. Microw. Theory Techn.*, vol. 66, no. 4, pp. 2010–2017, Apr. 2018.

[2] V. Vassilev, H. Zirath, R. Kozhuharov, and S. Lai, "140–220-GHz DHBT detectors," *IEEE Trans. Microw. Theory Techn.*, vol. 61, no. 6, pp. 2353–2360, Jun. 2013.

[3] Y. Campos-Roca, C. Schworer, A. Leuther, and M. Seelmann-Eggebert, "G-band metamorphic HEMT-based frequency multipliers," *IEEE Trans. Microw. Theory Techn.*, vol. 54, no. 7, pp. 2983–2992, Jul. 2006.

[4] V. K. Paidi, Z. Griffith, Y. Wei, M. Dahlstrom, M. Urteaga, N. Parthasarathy, M. Seo, L. Samoska, A. Fung, and M. J. W. Rodwell, "G-band (140–220 GHz) and W-band (75–110 GHz) InP DHBT medium power amplifiers," *IEEE Trans. Microw. Theory Techn.*, vol. 53, no. 2, pp. 598–605, Feb. 2005.

[5] J. Wu, Y. J. Cheng, and Y. Fan, "A wideband high-gain high-efficiency hybrid integrated plate array antenna for V-band inter-satellite links," *IEEE Trans. Antennas Propag.*, vol. 63, no. 4, pp. 1225–1233, Apr. 2015.

[6] D. Deslandes and K. Wu, "Integrated microstrip and rectangular waveguide in planar form," *IEEE Microw. Wireless Compon. Lett.*, vol. 11, no. 2, pp. 68–70, Feb. 2001.

[7] T. Li and Z. N. Chen, "Control of beam direction for substrate-integrated waveguide slot array antenna using metasurface," *IEEE Trans. Antennas Propag.*, vol. 66, no. 6, pp. 2862–2869, Jun. 2018.

[8] L. Wang, X. Yin, S. Li, H. Zhao, L. Liu, and M. Zhang, "Phase corrected substrate integrated waveguide H-Plane horn antenna with embedded metal-via arrays," *IEEE Trans. Antennas Propag.*, vol. 62, no. 4, pp. 1854–1861, Apr. 2014.

[9] T. Li and Z. N. Chen, "Wideband substrate-integrated waveguide-fed endfire metasurface antenna array," *IEEE Trans. Antennas Propag.*, vol. 66, no. 12, pp. 7032–7040, Dec. 2018.

[10] H. Jamshidi-Zarmehri and M. H. Neshati, "Design and development of high-gain SIW H-Plane horn antenna loaded with waveguide, dipole array, and reflector nails using thin substrate," *IEEE Trans. Antennas Propag.*, vol. 67, no. 4, pp. 2813–2818, Apr. 2019.

[11] Y. Zhang, W. Hong, and R. Mittra, "45 GHz wideband circularly polarized planar antenna array using inclined slots in modified short-circuited SIW," *IEEE Trans. Antennas Propag.*, vol. 67, no. 3, pp. 1669–1680, Mar. 2019.

[12] J. Xiao, Z. Qi, X. Li, and H. Zhu, "Broadband and high-gain SIW-fed slot array for millimeter-wave applications," *IEEE Trans. Antennas Propag.*, vol. 67, no. 5, pp. 3484–3489, May 2019.

[13] P. Liu, X. Zhu, Z. H. Jiang, Y. Zhang, H. Tang, and W. Hong, "A compact single-layer Q-band tapered slot antenna array with phase-shifting inductive windows for endfire patterns," *IEEE Trans. Antennas Propag.*, vol. 67, no. 1, pp. 169–178, Jan. 2019.

[14] J. Zhu, Y. Yang, S. Li, S. Liao, and Q. Xue, "Single-ended-fed high-gain LTCC planar aperture antenna for 60 GHz antenna-in-package applications," *IEEE Trans. Antennas Propag.*, vol. 67, no. 8, pp. 5154–5162, Aug. 2019.

[15] T. Li and Z. N. Chen, "Shared-surface dual-band antenna for 5G applications," *IEEE Trans. Antennas Propag.*, vol. 68, no. 2, pp. 1128–1133, Feb. 2020, doi: 10.1109/TAP.2019.2938584.

[16] J.-W. Lian, Y.-L. Ban, J.-Q. Zhu, J. Guo, and Z. Chen, "Planar 2-D scanning SIW multibeam array with low sidelobe level for millimeter-wave applications," *IEEE Trans. Antennas Propag.*, vol. 67, no. 7, pp. 4570–4578, Jul. 2019.

[17] N.-W. Liu, M.-J. Sun, L. Zhu, D. Xie, and G. Fu, "A low-profile printed cavity antenna with simultaneous bandwidth and radiation pattern improvement," *IEEE Antennas Wireless Propag. Lett.*, vol. 18, no. 10, pp. 2125–2129, Oct. 2019.

[18] J. Xu, Z. N. Chen, X. Qing, and W. Hong, "140-GHz planar broadband LTCC SIW slot antenna array," *IEEE Trans. Antennas Propag.*, vol. 60, no. 6, pp. 3025–3028, Jun. 2012.

[19] J. Xu, Z. N. Chen, X. Qing, and W. Hong, "140-GHz TE_{20}-mode dielectric-loaded SIW slot antenna array in LTCC," *IEEE Trans. Antennas Propag.*, vol. 61, no. 4, pp. 1784–1793, Apr. 2013.

[20] Z.-W. Miao, Z.-C. Hao, G. Q. Luo, L. Gao, J. Wang, X. Wang, and W. Hong, "140 GHz high-gain LTCC-integrated transmit-array antenna using a wideband SIW aperture-coupling phase delay structure," *IEEE Trans. Antennas Propag.*, vol. 66, no. 1, pp. 182–190, Jan. 2018.

[21] J. Xiao, X. Li, Z. Qi, and H. Zhu, "140-GHz TE_340-mode substrate integrated cavities-fed slot antenna array in LTCC," *IEEE Access*, vol. 7, pp. 26307–26313, 2019.

[22] D. Kim, J. Hirokawa, M. Ando, J. Takeuchi, and A. Hirata, "64×64-element and 32×32-element slot array antennas using double-layer hollow-waveguide corporate-feed in the 120-GHz band," *IEEE Trans. Antennas Propag.*, vol. 62, no. 3, pp. 1507–1512, Mar. 2014.

[23] P.-S. Kildal, "Three metamaterial-based gap waveguides between parallel metal plates for mm/submm waves," in *Proc. 3rd Eur. Conf. Antennas Propag. (EUCAP)*, Berlin, Germany, Mar. 2009, pp. 28–32.

[24] J. Liu, J. Yang, and A. U. Zaman, "Analytical solutions to characteristic impedance and losses of inverted microstrip gap waveguide based on variational method," *IEEE Trans. Antennas Propag.*, vol. 66, no. 12, pp. 7049–7057, Dec. 2018.

[25] M. Ferrando-Rocher, J. I. Herranz-Herruzo, A. Valero-Nogueira, and B. Bernardo-Clemente, "Performance assessment of gap-waveguide array antennas: CNC milling versus three-dimensional printing," *IEEE Antennas Wireless Propag. Lett.*, vol. 17, no. 11, pp. 2056–2060, Nov. 2018.

[26] J. Liu, A. Vosoogh, A. U. Zaman, and J. Yang, "A slot array antenna with single-layered corporate-feed based on ridge gap waveguide in the 60 GHz band," *IEEE Trans. Antennas Propag.*, vol. 67, no. 3, pp. 1650–1658, Mar. 2019.

[27] A. Vosoogh, "An E-band compact frequency division duplex radio front-end based on gap waveguide technology," in *Proc. 13th Eur. Conf. Antennas Propag. (EuCAP)*, Kraków, 2019, pp. 1–5.

[28] A. Vosoogh, A. Haddadi, A. U. Zaman, J. Yang, H. Zirath, and A. A. Kishk, "W-band low-profile monopulse slot array antenna based on gap waveguide corporate-feed network," *IEEE Trans. Antennas Propag.*, vol. 66, no. 12, pp. 6997–7009, Dec. 2018.

[29] A. Vosoogh, A. Uz Zaman, V. Vassilev, and J. Yang, "Zero-gap waveguide: A parallel plate waveguide with flexible mechanical assembly for mm-wave antenna applications," *IEEE Trans. Compon., Packag., Manuf. Technol.*, vol. 8, no. 12, pp. 2052–2059, Dec. 2018.

[30] J. I. H. Herruzo, A. Valero-Nogueira, S. M. Giner, and A. V. Jimenez, "Untilted narrow-wall slots excited by parasitic dipoles in groove gap waveguide technology," *IEEE Trans. Antennas Propag.*, vol. 63, no. 11, pp. 4759–4765, Nov. 2015.

[31] J. Liu, A. Uz Zaman, and J. Yang, "Design of wideband slot array antenna by groove gap waveguide in millimeter waves," in *Proc. IEEE-APS Topical Conf. Antennas Propag. Wireless Commun. (APWC)*, Cartagena des Indias, Colombia, Sep. 2018, pp. 725–728.

[32] Z. Talepour and A. Khaleghi, "Groove gap cavity slot array antenna for millimeter wave applications," *IEEE Trans. Antennas Propag.*, vol. 67, no. 1, pp. 659–664, Jan. 2019.

[33] J. L. Vazquez-Roy, A. Tamayo-Dominguez, E. Rajo-Iglesias, and M. Sierra-Castaner, "Radial line slot antenna design with groove gap waveguide feed for monopulse radar systems," *IEEE Trans. Antennas Propag.*, vol. 67, no. 10, pp. 6317–6324, Oct. 2019.

[34] A. Farahbakhsh, D. Zarifi, and A. U. Zaman, "60-GHz groove gap waveguide based wideband H-Plane power dividers and transitions: For use in high-gain slot array antenna," *IEEE Trans. Microw. Theory Techn.*, vol. 65, no. 11, pp. 4111–4121, Nov. 2017.

[35] D. Sun and J. Xu, "A novel iris waveguide bandpass filter using air gapped waveguide technology," *IEEE Microw. Wireless Compon. Lett.*, vol. 26, no. 7, pp. 475–477, Jul. 2016.

[36] D. Sun, X. Chen, J.-Y. Deng, L.-X. Guo, W. Cui, K. Yin, Z. Chen, C. Yao, and F. Huang, "Gap waveguide with interdigital-pin bed of nails for high-frequency applications," *IEEE Trans. Microw. Theory Techn.*, vol. 67, no. 7, pp. 2640–2648, Jul. 2019.

[37] Z. Liu, J.-Y. Deng, and D. Sun, "Slow-wave groove gap waveguide band-pass filter," *IEEE Access*, vol. 7, pp. 52581–52588, 2019.

[38] A. Vosoogh, H. Zirath, and Z. S. He, "Novel air-filled waveguide transmission line based on multilayer thin metal plates," *IEEE Trans. THz Sci. Technol.*, vol. 9, no. 3, pp. 282–290, May 2019.

HANGCHENG HAN received the B.S., M.S., and Ph.D. degrees in electrical engineering from the Beijing Institute of Technology, Beijing, China, in 2006, 2008, and 2012, respectively. He is currently with the School of Information and Electronics, Beijing Institute of Technology. His current research interests include resource allocation, interference suppression, and transceiver design.

XUHUI DING received the B.S. degree from the Beijing Institute of Technology, Beijing, China, in 2014, where he is currently pursuing the Ph.D. degree. His research interests include high data rate wireless communication, channel coding, iterative detection, and terahertz communication.

JINLIN LIU (Member, IEEE) received the B.Sc. degree in communications engineering from the University of Electronic Science and Technology of China (UESTC), Chengdu, China, in 2005, the Vordiploma from the Munich University of Technology, Munich, Germany, in 2011, the Swedish Licentiate degree in 2016, and the Ph.D. degree from the Chalmers University of Technology, Gothenburg, Sweden, in 2019. From 2005 to 2007, he was with Intel, Chengdu Branch, as a Test Engineer. From 2013 to 2014, he was with Eurodesign GmbH, Munich, as a PCB Test Engineer. His current research interests include fundamental electromagnetic theory, millimeter-wave planar antennas in general, gap waveguide technology, and frequency-selective surfaces. He received the Best Student Paper Award (first place) from the 2017 International Symposium on Antennas and Propagation, Phuket, Thailand. He serves on the reviewer board of several journals, including the IEEE TRANSACTIONS ON ANTENNAS AND PROPAGATION, the IEEE TRANSACTIONS ON MICROWAVE THEORY AND TECHNIQUES, the IEEE TRANSACTIONS ON COMPONENTS, PACKAGING, AND MANUFACTURING, the IEEE ANTENNAS AND WIRELESS PROPAGATION LETTERS, the IEEE MICROWAVE AND WIRELESS COMPONENTS LETTERS, and *Journal of Electromagnetic Waves and Applications*.

JIANPING AN (Member, IEEE) received the Ph.D. degree from the Beijing Institute of Technology, China, in 1996. He joined the School of Information and Electronics, Beijing Institute of Technology, in 1995, where he is currently a Full Professor and also the Dean of the School of Information and Electronics. His research interests are in the field of digital signal processing, cognitive radio, wireless networks, and high-dynamic broadband wireless transmission technology.

XIANGYUAN BU received the B.Eng. and Ph.D. degrees from the Beijing Institute of Technology, Beijing, China, in 1987 and 2007, respectively. From 1996 to 1998, he was a Visiting Scholar with the Military Academy of Belarus, Belarus. Since 2002, he has been with the School of Information and Electronics, BIT, where he is currently a Professor. His current research interests include wireless communication, digital signal processing, and channel coding.

ZHONGXIA SIMON HE (Senior Member, IEEE) received the M.Sc. degree from the Beijing Institute of Technology, Beijing, China, in 2008, and the Ph.D. degree from the Chalmers University of Technology, Göteborg, Sweden, in 2014.

He is currently an Assistant Professor with the Microwave Electronics Laboratory, Department of Microtechnology and Nanoscience (MC2), Chalmers University of Technology. His current research interests include high data rate wireless communication, modulation and demodulation, mixed-signal integrated circuit design, radar, and packaging.

● ● ●